International Journal of Nanomedicine

Dovepress
open access to scientific and medical research

Open Access Full Text Article

ORIGINAL RESEARCH

The influence of direct laser metal sintering implants on the early stages of osseointegration in diabetic mini-pigs

This article was published in the following Dove Press journal:
International Journal of Nanomedicine
31 July 2017
Number of times this article has been viewed

Naiwen Tan[1–3,*]
Xiangwei Liu[1,2,*]
Yanhui Cai[4]
Sijia Zhang[1,2]
Bo Jian[1,2]
Yuchao Zhou[1,2]
Xiaoru Xu[1,2]
Shuai Ren[1,2]
Hongbo Wei[1,2]
Yingliang Song[1,2]

[1]State Key Laboratory of Military Stomatology, National Clinical Research Center for Oral Diseases, Shaanxi Engineering Research Center for Dental Materials and Advanced Manufacture, Xi'an, Shaanxi, China; [2]Department of Implant Dentistry, School of Stomatology, The Fourth Military Medical University, Xi'an, Shaanxi, China; [3]Department of Stomatology, Hospital 463 of PLA, Xi'an, Shaanxi, China; [4]Department of Anesthesiology, Xijing Hospital, The Fourth Military Medical University, Xi'an, Shaanxi, China

*These authors contributed equally to this work

Background: High failure rates of oral implants have been reported in diabetic patients due to the disruption of osseointegration. The aim of this study was to investigate whether direct laser metal sintering (DLMS) could improve osseointegration in diabetic animal models.

Methods: Surface characterizations were carried out on two types of implants. Cell morphology and the osteogenic-related gene expression of MG63 cells were observed under conditions of DLMS and microarc oxidation (MAO). A diabetes model in mini-pigs was established by intravenous injection of streptozotocin (150 mg/kg), and a total of 36 implants were inserted into the mandibular region. Micro-computed tomography (micro-CT) and histologic evaluations were performed 3 and 6 months after implantation.

Results: The Ra (the average of the absolute height of all points) of MAO surface was 2.3±0.3 μm while the DLMS surface showed the Ra of 27.4±1.1 μm. The cells on DLMS implants spread out more podia than those on MAO implants through cell morphology analysis. Osteogenic-related gene expression was also dramatically increased in the DLMS group. Obvious improvement was observed in the micro-CT and Van Gieson staining analyses of DLMS implants compared with MAO at 3 months, although this difference disappeared by 6 months. DLMS implants showed a higher bone–implant contact percentage (33.2%±11.2%) at 3 months compared with MAO group (18.9%±7.3%) while similar results were showed at 6 months between DLMS group (42.8%±10.1%) and MAO group (38.3%±10.8%).

Conclusion: The three-dimensional environment of implant surfaces with highly porous and fully interconnected channel and pore architectures can improve cell spreading and accelerate the progress of osseointegration in diabetic mini-pigs.

Keywords: laser manufacturing, dental implants, diabetes mellitus, osseointegration

Introduction

Today, dental implants have been considered as a well-accepted treatment modality for replacing missing teeth. Close contact between bones and implants (osseointegration) is considered to be the foundation of implant success. Osseointegration starts with fibrin clot extending around the screw rapidly after the insert of implant and then osteoblasts attach to the surface of implant. During this period, a series of complex bone remodeling processes happen around the implant including osteogenesis and bone resorption. Finally, a close relation forms between bone and implant connected by collagenous filaments and this direct bone anchorage provides long-term function of implant.[1–3] However, a high failure rate is observed in patients with diabetes mellitus (DM).[4] Researchers have reported implant a much higher failure rates ranging from 20% to 10% in diabetic patients than that of 1%–3% in normal patients.[5,6]

Correspondence: Yingliang Song
Department of Implant Dentistry, School of Stomatology, Fourth Military Medical University, 145 West Changle Road, Xi'an 710032, People's Republic of China
Tel +86 029 8477 6454
Email yingliangsong@163.com

submit your manuscript | www.dovepress.com
Dovepress
http://dx.doi.org/10.2147/IJN.S138615

Some other studies reported implant success rates ranging from 85.6% to 94.3% in diabetic patients.[7] Systemic complications caused by diabetes, including retinopathy, nephropathy, and neuropathy, can cause a systemic inflammatory response. Excess inflammatory cytokines restrict osteoblast differentiation and proliferation and stimulate mononuclear macrophage to differentiate into osteoclast.[8] This process results in the destruction of bone tissue. Moreover, the high blood glucose levels in patients with diabetes change the microenvironment around implants, reduce wound healing, and disturb the early stages of osseointegration.[9,10] All of these issues may be related to the formation of advanced glycation end products (AGEs), which are considered to have a significant impact on the pathogenesis of diabetes. AGEs disturb cell growth, adhesion, and differentiation and cause the accumulation of extracellular matrix in the osseointegration process, which reduces the implant success rate in diabetic patients.[11,12]

Dental implants are usually made of titanium because of its good mechanical properties, including excellent ductility, corrosion resistance, low modulus of elasticity, and biocompatibility.[13] However, commercially pure titanium lacks the capacity to induce osteoblast growth and cannot stimulate bone formation surrounding an implant because of its inert surface. Appropriate modification of the implant surfaces can promote better and faster implant osseointegration and stability, and such modifications also improve the bone histocompatibility of implants and the capacity for osteogenesis.[14–16] Thus, modifications to the implant surface geometry are very important for patient outcomes. In particular, studies have shown that rough surfaces can improve bone apposition and osteoconductivity more effectively than smooth surfaces, and surface roughness influences fibrin clot retention and is important for the early stages of osseointegration.[17,18] Recently, with the development of three-dimensional (3D) printing technology, a new implant made by direct laser fabrication (DLF) broadened the field of implant manufacturing. As a new manufacturing technique, DLF has been widely used in the medical domain for biocompatible orthopedic implants, dental implants, and 3D reconstruction plates used in bony defects.[19–21] Using direct laser metal sintering (DLMS) technology, these new dental implants with different shapes and textures can be fabricated by the laser fusion of titanium microparticles under 3D computer-aided design.[22] The surfaces and interconnections of DLMS implants with a pore depth of 200–300 μm were reported to be optimal for osteoblast ingrowth and differentiation,[23] likely because these complicated surfaces can provide an increased contact area with better contact positioning for osteoblasts.

In this study, mini-pigs were chosen as an animal model for diabetes induction in which we could observe the contact between bone and implant following implant placement in the mandibular region. Due to the anatomical, physiological, and metabolic similarities with human body, mini-pigs are considered as a suitable model in biomedical research.[24] The common blood biochemical index of mini-pigs and the absorption, transfer, and utilization of glucose are also similar to the corresponding processes in humans.[25] Thus, mini-pigs can be considered a valuable model for observing bone remodeling and the interaction between bone and implants under the impact of diabetes.

We aimed to investigate the acceleration of osseointegration in diabetes mini-pigs caused by DLMS implants. The surface characteristics and the influence of implant surface to the osteoblast behavior were compared between DLMS implants and microarc oxidation (MAO) implants in vitro. The 3D environment of DLMS implant could promote cells to spread out on its surface, and accelerate the process of osseointegration in diabetes mini-pigs. It could provide a new way to improve the implant success rate in diabetes patients.

Materials and methods

Implants preparation

All of the test implants were prepared with DLMS surface technology. The specification and characterization of the DLMS process were performed as described previously.[22] The manufacturing processing of DLMS implants was performed using a powerful ytterbium fiber laser system (EOS GmbH, Munchen, Germany) with a scanning rate of 7 m/s and a power of 200 W in an argon atmosphere. The implants were washed in distilled water in a sonic bath for 5 min, then immersed in sodium hydrate (20 g/L) and hydrogen peroxide (20 g/L) for 30 min, and ultrasonically cleaned in distilled water for 5 min again to remove residual particles produced from the manufacturing process. Then, the DLMS implants underwent acid etching to remove weakly adherent particles. This process was conducted by immersing the samples in a mixture of 50% maleic acid and 50% oxalic acid for 45 min, followed by sonication in distilled water for 5 min. Then, the samples were immersed in 65% aqueous nitric acid for 30 min and were ultrasonically cleaned in distilled water.

MAO implants were prepared for the control group. As described previously, the manufacturing process of MAO implants was performed.[26] The samples were anodized in the electrolyte solution for 5 min at a voltage of 400 V.

The electrolytes included calcium acetate monohydrate (0.2 M) and β-glycerophosphate disodium salt pentahydrate (0.02 M). Then, the samples were sonicated with distilled water for 10 min and dried under air flow. Finally, the samples were submitted to ultraviolet irradiation to form abundant hydroxyl. All of the implants were sterilized in an autoclave at 114°C for 20 min before surgery.

Morphological analysis of the surfaces

Surface characterization of two different implants was observed under 3D surface topography instrument (NANOVEA PS50; Nanovea, Irvine, CA, USA). Three DLMS and three MAO implants were used for morphological analysis, and scanning areas were chosen randomly on three different areas of the implant surface. The roughness values were obtained from the 3D reconstructions of the scanning areas.

Cell culture and seeding

The MG63 cell line (human osteosarcoma cell line, obtained from Chinese Academy of Sciences, Shanghai Cell Bank) was maintained in Dulbecco's Modified Eagle's Medium (DMEM) and contained 100 g/mL streptomycin (Sigma-Aldrich, St Louis, MO, USA), 100 U/mL penicillin, and 10% fetal bovine serum (Gibco, Waltham, MA, USA), and cells were cultured in a humidified atmosphere of 5% CO_2 at 37°C. The medium was replaced every 3 days, and MG63 cells were passaged upon reaching 80% confluency.

Cell morphology

The MG63 cells (2×10^5/mL) were seeded onto the surface of the implants for 4 hours and then soaked and cultured in the DMEM medium for 4 hours. After that, the implants with cells incubated on them were washed with PBS (Gibco) for three times, then fixed in 2% glutaraldehyde for 10 min, dehydrated in a graded ethanol series and freeze-dried after 24 hours of incubation post-transfection. We observed the cell morphology by field emission scanning electron microscopy (FE-SEM), after the samples were sputter-coated with gold.

Osteogenic-related gene expression

The MG63 cells were seeded onto the surface of the implants, the osteogenic induction of MG63 cells was performed when the cells reached 80% confluence. The osteogenic induction of MG63 cells was performed in an osteogenic medium supplemented with 50 mg/mL ascorbic acid, 10^{-7} M dexamethasone, and 10 mM β-glycerophosphate. Total ribonucleic acid (RNA) of the MG63 cells was extracted with TRIzol reagent 5 and 10 days after induction. Then, 1 μg of total RNA quantified by optical density measurement was subjected to reverse transcription to yield complementary deoxyribonucleic acid (cDNA) with the PrimeScript™ RT reagent kit after the RNA samples were treated with DNAse. Normalized cDNA was amplified in an Applied Biosystems 7500 Real-Time PCR System with the SYBR Premix Ex™ Taq II RT-PCR kit, and the related primer sequences with high specific advantage were as follows (forward/reverse): COL (CAAGGTGTTGTGCGATGACG/TGGTTTCTTG GTCGGTGGG), RUNX2 (ACCTGAGCCAGATGACG/ CAGTGAGGGATGAAATGC), ALP (CCCCTGAGCG TCCTGTTCT/GGCGGCAGACTTTGGTTTC). After the fluorescence reached a threshold, the cycle number was recorded. β-actin was used as an endogenous reference. The messenger RNA expression was calculated and defined as the 2-delta delta Ct.

Animals

Six mini-pigs were used in this study. The animals were all 6 months old (20.97±1.26 kg) at the beginning of the study. Feeding and housing were performed according to standard animal care protocols. The experimental protocol was approved by the Ethics Committee of the Forth Military Medical University and performed in accordance with ethical guidelines (Ethics Approval Number: 2015 kq-022 #) of Animal Welfare Committee of the Fourth Military Medical University. All of the surgical procedures and the induction of diabetes were performed under systemic and local anesthesia. Ceftazidime (100 mg/kg; Pharmaceutical Department, School of Stomatology, The Forth Military Medical University) was applied intramuscularly before and 2 days after the operation.

The induction of diabetes mellitus

For the induction of diabetes, streptozotocin (STZ) (150 mg/kg; Parc d' Innovation, BP 50067, lllkirch Cedex, France) was dissolved in saline (1 g/10 mL) and injected into the mini-pigs via an ear vein over a period of 20 min, as described previously.[27] To meet the criteria set by the World Health Organization for diabetes and to define diabetes, the fasting blood glucose level was measured, and an intravenous glucose tolerance test (IvGTT) was performed.

Blood glucose level and IvGTT

A glucose control strip (ACCU-CHEK® Mobile; Roche, Shanghai, China) was used to measure the fast blood glucose level with capillary blood from the ear. The measurement was performed before the morning meal to ensure the mini-pigs

had an empty stomach. The fasting blood glucose was measured every day in the first week after the induction of diabetes and was measured twice a week thereafter until the end of the experiment. An IvGTT was conducted 4 weeks after the induction of diabetes. The blood glucose levels of the animals were measured 10 min before and 10, 30, 60, and 120 min after glucose (1 g/kg, dissolved in saline) was injected via an ear vein.

Implant surgery

All the premolars on both sides of the mandibular were extracted 2 months after the induction of DM. After 6 months of healing, a total of 36 implants were inserted into the bone by one operator (Figure 1). Twenty-four of them were prepared with DLMS technology and the other 12 were prepared with MAO. The surgical sites were located in the mandible premolar regions. Each side of the mandibular received one MAO implant and two DLMS implants. The implants inserted into the right mandible were all retrieved after 3 months, and the others were retrieved after 6 months. All of the implants with surrounding tissue were recovered with a trephine bur and were immersed in 4% neutral formalin immediately after washing in a saline solution.

Tomography and histologic analyses

To evaluate the histological changes in the tissues around the implants, the specimens were observed under micro-computed tomography (micro-CT; Yxlon, Hamburg, Germany). All the specimens were scanned at a resolution of 12 μm, under the following parameters: 90 kV, 50 μA, 720 views. All the scanning data were analyzed in 3D modeling software (VGStudio MAX, Volume Graphics, Germany). The region of interest was chosen as 0.2 mm around the implants. The bone volume-to-tissue volume (BV/TV), trabecular number (Tb.N), trabecular thickness (Tb.Th), and trabecular separation (Tb.Sp) values were calculated based on the 3D reconstruction results.

All the implants were then fixed in formalin, decalcified, and inset in resin. The specimens (300 μm in thickness) were sectioned across the implants, using a high-precision diamond disk (Leica SP 1600; Leica, Wetzlar, Germany) and were ground to about 100 μm in thickness with a micro-grinder (RF-1; Rui-Feng Equipment, Xi'an, China). Three slices were obtained from each implant. Tissue slices were stained using the standard Van Gieson (VG) dying method and examined under a stereomicroscope (DMI6000 B; Leica Microsystems, Shanghai, China). The bone–implant contact rate (BIC%) was analyzed by a software program (Leica Imaging System, Cambridge, England). The circumference of the implant (B) and the length of the interface which implant directly contacted the bone tissues (A) were measured and the BIC% was calculated according to the formula below:

$$\text{Bone–implant contact \%} = A/B \times 100\%$$

The BIC% of each implant was represented by the mean of three slices.

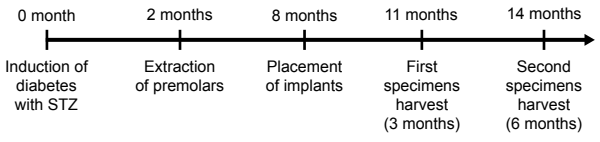

Figure 1 Chronological sequence of the implant surgery.
Abbreviation: STZ, streptozotocin.

Statistical analysis

All the measurements were carried out by one examiner who was masked with the identity of the specimens being evaluated. All the data were expressed as mean ± standard error. Statistical significance was determined with Student's *t*-test or one-way analysis of variance using SPSS software. Significance is considered at $P<0.05$.

Results

Surface characterization

All the selected areas on the same technologic surface showed no difference under 3D surface topography instrument. The 3D reconstruction images are shown in Figure 2. Obvious difference can be observed between two different surfaces. An extremely irregular and rough surface was shown on DLMS implants while MAO implants showed a relatively flat with uniform embossments surface. The Ra (the average of the absolute height of all points) of MAO surface was 2.3±0.3 μm while the DLMS surface showed the Ra of

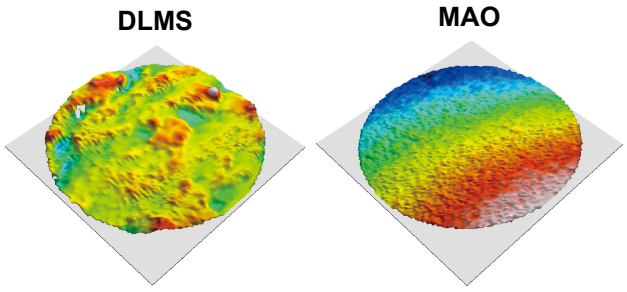

Figure 2 The three-dimensional reconstruction images of DLMS and MAO surface. The surface texture is readily evident after reconstruction.
Abbreviations: DLMS, direct laser metal sintering; MAO, microarc oxidation.

27.4±1.1 μm. The surface roughness evaluation of DLMS implants was difficult and the result may not realistically reflect the rough surface due to the fact that the presence of microspheres and channels cannot be scanned completely.

Cell morphology

We observed the cell morphology by FE-SEM (Figure 3). Generally, the cell morphology of DLMS implants was very similar to that of the cells grown on the MAO surface. Only a small portion of cells showed stretched out podia, and the number of podia for such cells was few. The cells with abundant filopodia and lamellipodia bridged over the rough surface of the DLMS implants and anchored themselves to the implants via the cell podia.

Osteogenic-related gene expression

Osteogenic-related genes, including runt-related transcription factor 2 (RUNX2), alkaline phosphatase (ALP), and

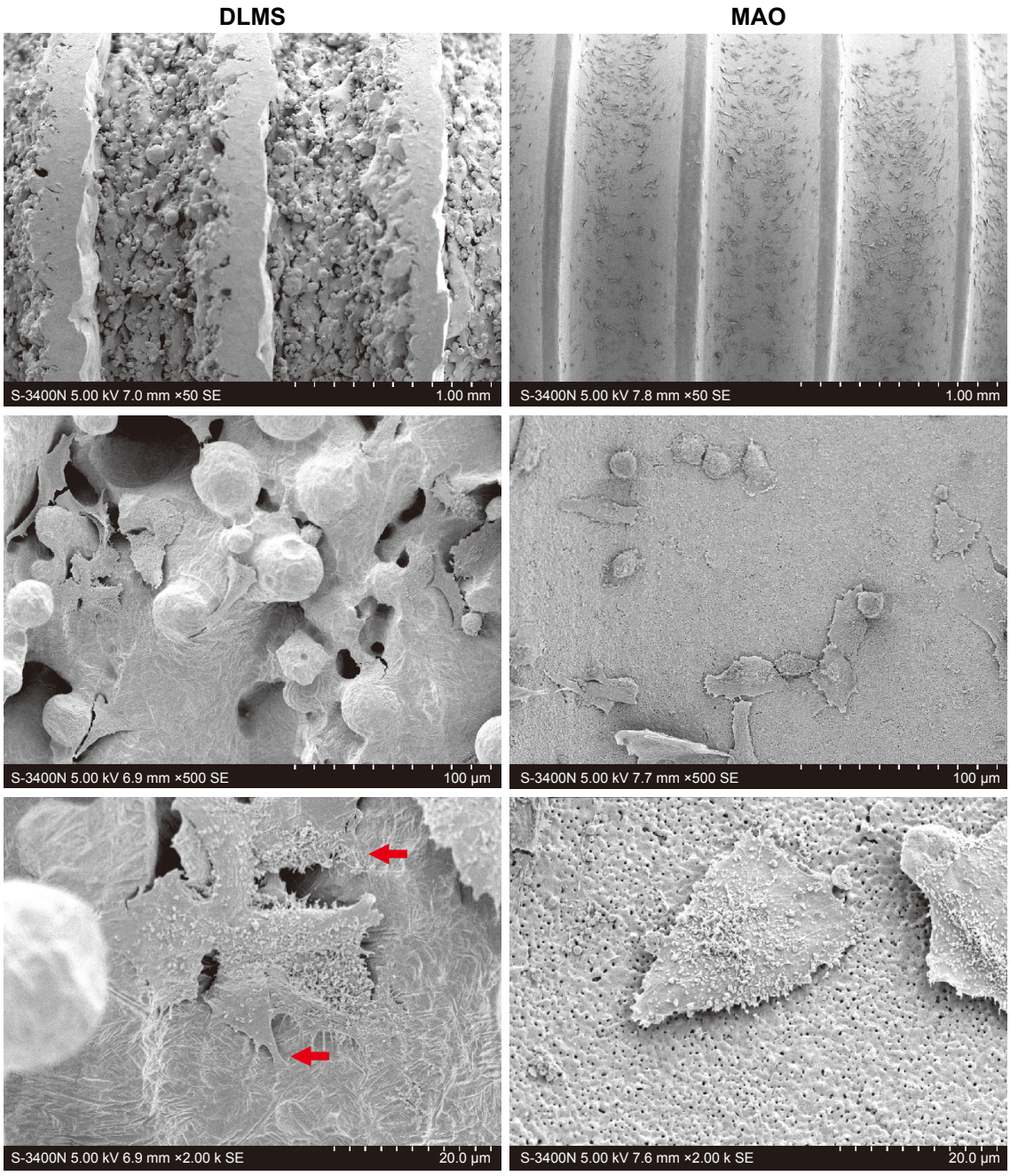

Figure 3 Cell morphology observed by field emission scanning electron microscopy after the cells cultured on DLMS and MAO implant for 4 hours.
Notes: Red arrows show the cell podia on DLMS implant surfaces. N=5.
Abbreviations: DLMS, direct laser metal sintering; MAO, microarc oxidation.

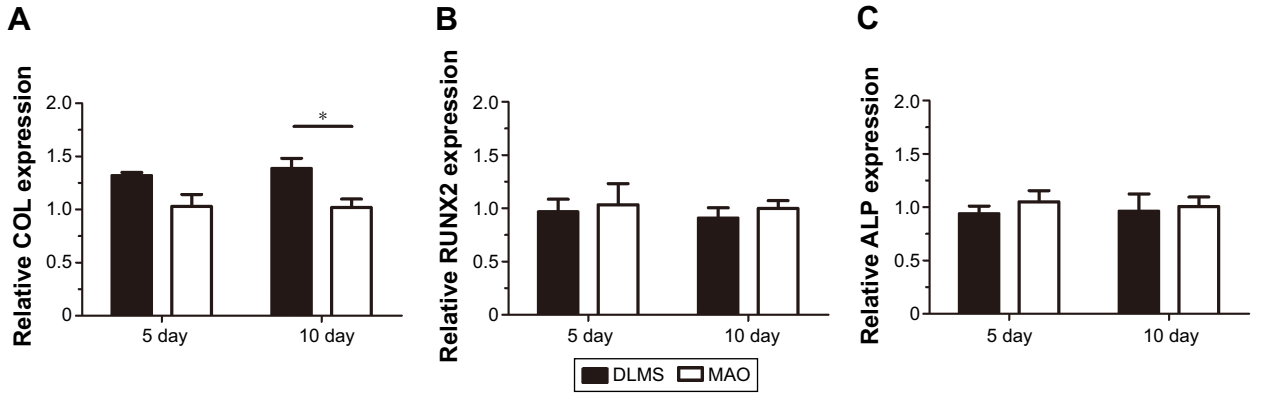

Figure 4 After osteogenic induction periods of 5 and 10 days, osteogenic-related gene expression was quantified by real-time quantitative polymerase chain reaction. COL, RUNX2, and ALP are shown in **A**–**C**, respectively. *$P<0.05$, N=5.
Abbreviations: ALP, alkaline phosphatase; COL, collagen; DLMS, direct laser metal sintering; MAO, microarc oxidation; RUNX2, runt-related transcription factor 2.

collagen (COL), were determined separately by real-time quantitative polymerase chain reaction at day 5 and day 10 following the osteogenic induction of MG63 cells. Each of these three related genes showed higher levels for the DLMS implant surfaces (Figure 4). Specifically, COL was significantly elevated on DLMS surfaces compared with MAO implant surfaces at day 10. No obvious difference was observed between the other groupings, although the osteogenic-related genes on the DLMS implant surfaces were expressed at higher levels as a whole.

Blood glucose level and IvGTT

Measurements of the fasting blood glucose level are shown in Figure 5A. The blood glucose level rapidly increased to over 20 mmol/L within 10 min of STZ injection. This level subsequently decreased to 10 mmol/L and stabilized 1 day after the induction of diabetes. The blood glucose level remained at ~10 mmol/L at 6 months after the induction of diabetes.

The blood glucose levels measured in the IvGTT are shown in Figure 5B. The blood glucose level rapidly increased to over 30 mmol/L within 10 min after the injection of glucose and remained at a high level (over 20 mmol/L) 2 hours after the injection.

Micro-computed tomography and histologic evaluation

The 3D reconstructions of two different implants with new bone around are shown in Figure 6. The micro-CT images showed that the new bone around MAO implant was obviously less than that around DLMS implant 3 months after implantation, while both types of implants showed similar bone growth at 6 months. The BV/TV, Tb.N, Tb.Th, and Tb.Sp values are shown in Figure 7, respectively. Significant differences were observed in the BV/TV, Tb.Th, and Tb.Sp values between the DLMS and MAO implants at 3 months after placement. However, this difference in BV/TV and Tb.Th values was lost at 6 months after placement.

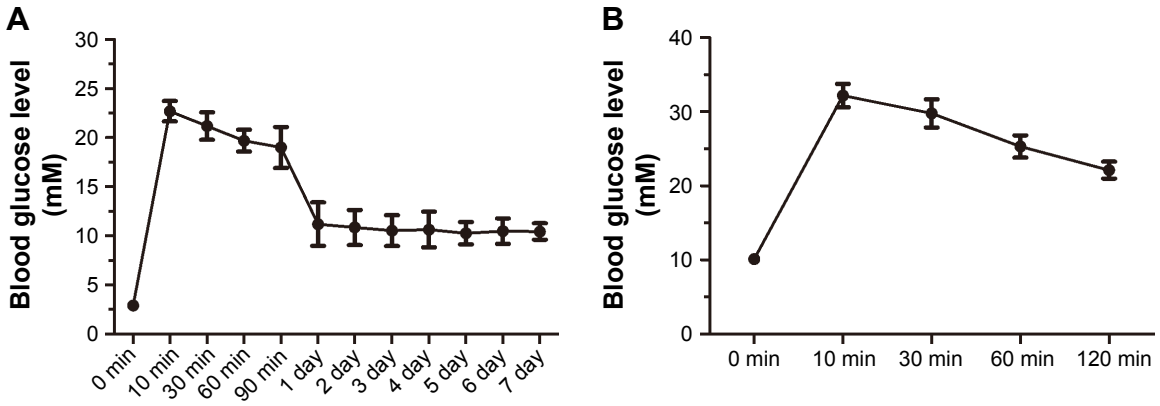

Figure 5 The change in the blood glucose level induced by diabetes mellitus based on the intravenous glucose tolerance test.
Notes: The fasting blood glucose level stabilized at 10 mmol/L 1 day after the induction (**A**). During the intravenous glucose tolerance test, the blood glucose level remained high for over 2 hours (**B**).

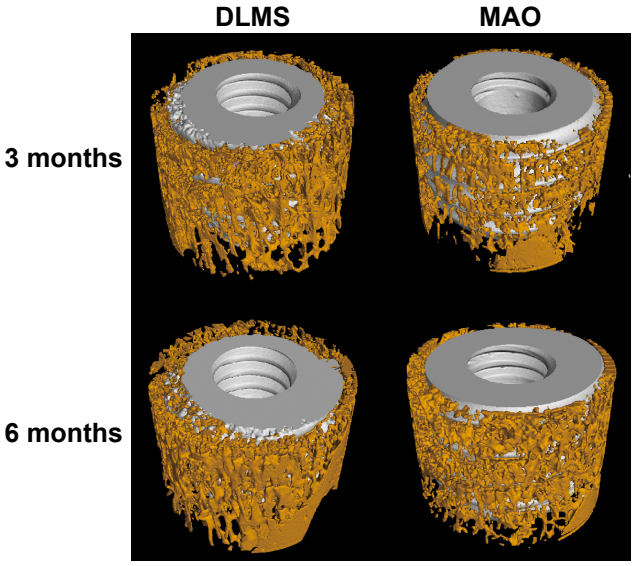

Figure 6 Micro-computed tomography analysis of osteogenesis of DLMS and MAO implant 3 and 6 months after surgery. This shows the three-dimensional reconstruction of the samples.
Abbreviations: DLMS, direct laser metal sintering; MAO, microarc oxidation.

No significant difference between groups was observed in Tb.N at 3 or 6 months after placement.

VG staining demonstrated contact between the implants and new bone (Figure 8). DLMS samples showed closer contact between implants and bone at both 3 months (Figure 8A) and 6 months (Figure 8C). In the MAO implants at month 3, we noted a layer of fibrovascularization tissue surrounding the implants, which separated the new bone from the implants (Figure 8B). The bone and implants were in direct contact by 6 months after placement of MAO samples (Figure 8D), and no significant differences were observed compared with the DLMS samples.

The BIC% results are shown in Figure 9. At 3 months, the BIC was 33.2%±11.2% in the DLMS group, which was significantly higher than 18.9%±7.3% observed in MAO groups. At 6 months, the BIC of both groups had different degrees of growth. The BIC in the DLMS group (42.8%±10.1%) was still a little higher than that in the MAO group (38.3%±10.8%) but this difference showed no significance.

Discussion

In the present study, we demonstrate that the surface resulted from DLF is conducive to cell spreading. Our results also suggest that implant with porous surface can accelerate osseointegration process in diabetic animal models.

All the DLMS specimens showed an extremely rough surface compared with the MAO specimens. Modification of implant surfaces can improve the biological behavior around implants and can accelerate the process of osseointegration.[28] The roughness and shape of the cavities

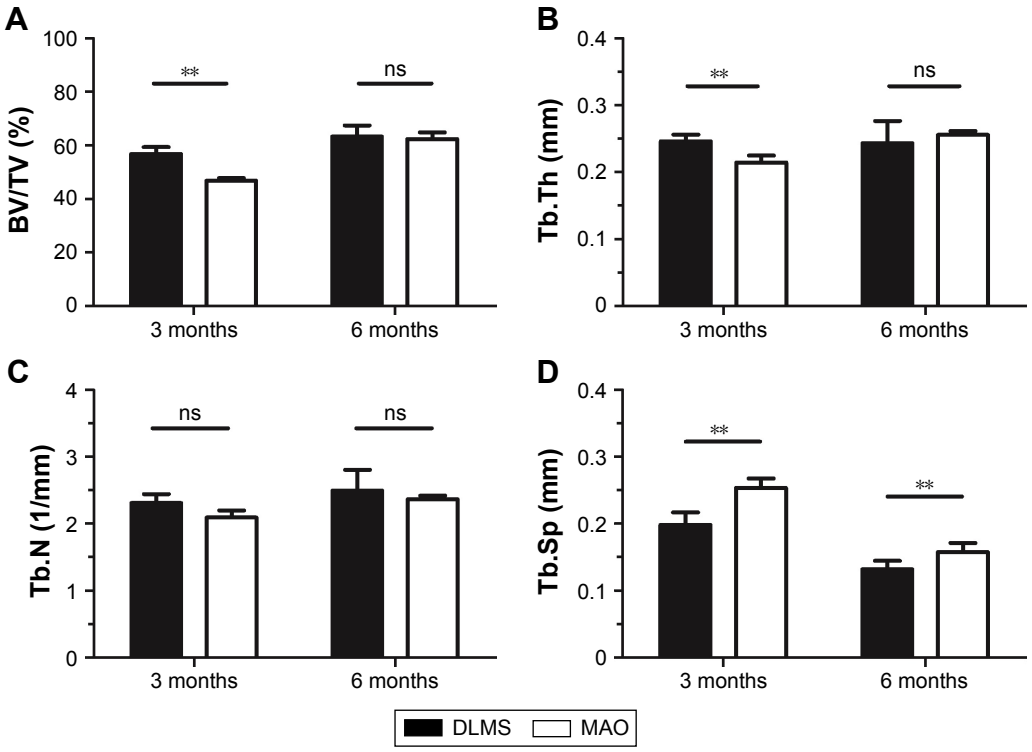

Figure 7 After rebuilding and analyzing, the BV/TV, Tb.Th, Tb.N, and Tb.Sp were measured; the results are shown in this figure. $^{**}P<0.01$.
Abbreviations: BV/TV, bone volume-to-tissue volume; DLMS, direct laser metal sintering; MAO, microarc oxidation; ns, no significant difference between two groups; Tb.N, trabecular number; Tb.Sp, trabecular separation; Tb.Th, trabecular thickness.

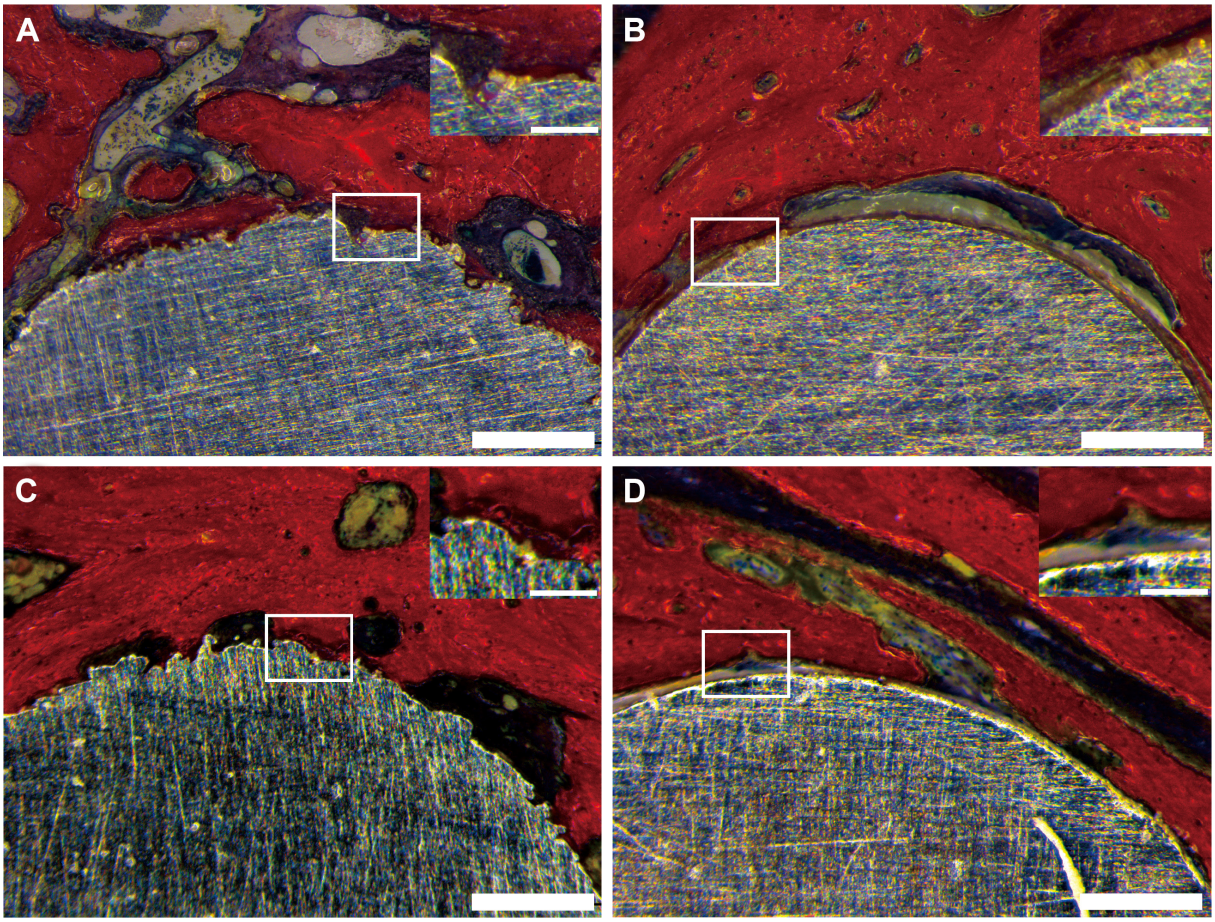

Figure 8 This figure shows the Van Gieson staining of the samples.
Notes: Direct laser metal sintering samples are shown in **A** and **C**. Microarc oxidation samples are shown in **B** and **D**. **A** and **B** show samples acquired at 3 months. **C** and **D** show samples acquired at 6 months. Scale bars =500 μm.

have been demonstrated to influence the differentiation of osteoblast cell.[29] Previous studies found that bones prefer to grow in pores depth of 100–400 μm.[30] Mangano et al[31] investigated the biological response of direct metal laser sintering implant surfaces in vitro. Stem cells rapidly differentiated into osteoblasts and endotheliocytes, as a result bone tissue can be produced along the implant surfaces.[31] Ingrowth of bone tissue into the porous structure makes it adhere to implant tightly. This anchoring structure is considered critical for a porous implant to achieve successful osseointegration. Implants manufactured by DLMS with characteristics of graded elasticity have also been shown to transfer stress from implants to the bone more naturally.[32]

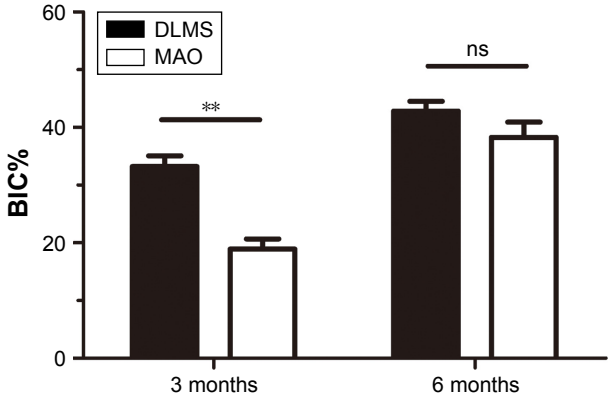

Figure 9 This Figure shows the BIC% of each group. **$P<0.01$.
Abbreviations: BIC%, bone–implant contact rate; DLMS, direct laser metal sintering; MAO, microarc oxidation; ns, no significant difference between two groups.

In this study, the MG63 cell line was cultured on DLMS and MAO implants. We found that cells on DLMS implants spread out more podia than those on MAO implants, and these abundant podia enabled the cells to tightly anchor themselves to the implant surfaces. This close contact between cells and the implant surface is important for the differentiation and proliferation of osteoblasts. Cells can spread over pores diameter smaller than a cell body (about 30 μm), but can grow into cavities of greater dimensions.[33] Our study showed the same result that cells grew into and adopted with the porous surface of DLMS implants, but tiled on the MAO surface with pores size about 0.5–2 μm. Previous studies have

reported similar results, showing that osteoblasts were able to migrate and proliferate on a DLMS-generated titanium surface.[34] These processes can accelerate the early stages of osseointegration, which is particularly important in diabetic patients, because high blood glucose levels reduce osseointegration by influencing the adhesion and growth of osteoblasts. Thus, our results indicate that rough implant surfaces may improve osseointegration in diabetic patients.

The osteogenic-related gene expression results showed that cells on DLMS implants had considerable expression levels of ALP, COL, and RUNX2, which demonstrates that osteoblasts can differentiate to bone tissue rapidly after attaching to the implant surface. However, no significant difference was observed between the DLMS and MAO implants, which may indicate that the influence of the rough implant surfaces on osseointegration did not improve osteogenic-related gene expression. Ingber claimed that 3D structure could force cells to adopt within and create mechanical stresses that regulate gene expression.[35] Previous studies also demonstrated that osteoblasts displayed comparable osteogenic-related gene expression on boss DLMS and acid-etched implants.[31]

The micro-CT results identified a significant difference between DLMS and MAO implants at 3 months postimplantation. The osseointegration around DLMS implants was clearly better than that around MAO implants. The BV/TV, Tb.Th, and Tb.Sp values were significantly better for the new bone around DLMS implants, suggesting that on DLMS surfaces, both bone quality and quantity can be improved in a shorter time period. This difference between DLMS and MAO implants was lost by 6 months postimplantation, which shows that osseointegration can be enhanced as healing time is prolonged. The significant difference in Tb.Sp between DLMS and MAO implants at 6 months is important to the long-term benefit in implant success. A poor Tb.Sp may cause patients suffer from bone absorption and fracture more easily. The improvement of Tb.Sp around DLMS implants could reduce the risk of fracture and bone absorption. This may be important to the bone tissue not only around implants but also in the other parts of body like spine. VG staining and BIC% results showed similar results to the micro-CT analysis. The fibrovascularization tissue observed around MAO implant surfaces at 3 months postimplantation demonstrated poor osseointegration. Thus, MAO implant surfaces require a longer time to complete the early stages of osseointegration in diabetic patients, while the DLMS implants achieved better osseointegration in the same period. For the DLMS surfaces, new bone formation was primarily accomplished within the first 3 months; however, it took 6 months for MAO implants to demonstrate a similar effect. The difference of BIC% in two groups at 6 months may be because the extremely rough surface of DLMS implant increased the contact area between the implant and bone. Previous studies also reported a higher osseointegration in DLMS implants than that in machined implants and a faster bone formation within the cavities of DLMS implant surface.[36] It may be because a higher roughness surface could provide a better environment for fibrin clot stability and accelerating the progress of bone healing on the implant surface. Osseointegration at the bone-to-implant interface is influenced by several mechanisms including osteoblasts adhesion, proliferation, and bone deposition. All these mechanisms might be affected by different modifications of implant surface.

Conclusion

This study demonstrates that cells are more spread out on DLMS implants than on MAO implants. DLMS implant with highly porous and fully interconnected channel and pore surface may accelerate the process of osseointegration in diabetic mini-pigs. However, if the healing time is sufficient, the osseointegration on MAO implant surfaces was identical to that on DLMS implants. Future studies should focus on whether the osseointegration on DLMS implant surfaces differs between diabetic patients and healthy controls.

Acknowledgment

This work is supported by grants from the Nature Science Foundation of China (NSFC; grant numbers 81170984 and 81470775).

Disclosure

The authors report no conflicts of interest in this work.

References

1. Branemark PI, Adell R, Breine U, Hansson BO, Lindstrom J, Ohlsson A. Intra-osseous anchorage of dental prostheses. I. Experimental studies. *Scand J Plast Reconstr Surg*. 1969;3(2):81–100.
2. Albrektsson T, Branemark PI, Hansson HA, Lindstrom J. Osseointegrated titanium implants. Requirements for ensuring a long-lasting, direct bone-to-implant anchorage in man. *Acta Orthop Scand*. 1981;52(2):155–170.
3. Le Guehennec L, Soueidan A, Layrolle P, Amouriq Y. Surface treatments of titanium dental implants for rapid osseointegration. *Dent Mater*. 2007;23(7):844–854.
4. Karoussis IK, Kotsovilis S, Fourmousis I. A comprehensive and critical review of dental implant prognosis in periodontally compromised partially edentulous patients. *Clin Oral Implants Res*. 2007;18(6):669–679.
5. Javed F, Romanos GE. Impact of diabetes mellitus and glycemic control on the osseointegration of dental implants: a systematic literature review. *J Periodontol*. 2009;80(11):1719–1730.

6. Kotsovilis S, Karoussis IK, Fourmousis I. A comprehensive and critical review of dental implant placement in diabetic animals and patients. *Clin Oral Implants Res*. 2006;17(5):587–599.
7. Courtney MW Jr, Snider TN, Cottrell DA. Dental implant placement in type II diabetics: a review of the literature. *J Mass Dent Soc*. 2010; 59(1):12–14.
8. McCarthy AD, Uemura T, Etcheverry SB, Cortizo AM. Advanced glycation endproducts interefere with integrin-mediated osteoblastic attachment to a type-I collagen matrix. *Int J Biochem Cell Biol*. 2004; 36(5):840–848.
9. Pfeffer MA, Burdmann EA, Chen CY, et al; TREAT Investigators. A trial of darbepoetin alfa in type 2 diabetes and chronic kidney disease. *N Engl J Med*. 2009;361(21):2019–2032.
10. von Wilmowsky C, Stockmann P, Metzler P, Harsch IA, Amann K, Schlegel KA. Establishment of a streptozotocin-induced diabetic domestic pig model and a systematic evaluation of pathological changes in the hard and soft tissue over a 12-month period. *Clin Oral Implants Res*. 2010;21(7):709–717.
11. Tolosa MJ, Chuguransky SR, Sedlinsky C, et al. Insulin-deficient diabetes-induced bone microarchitecture alterations are associated with a decrease in the osteogenic potential of bone marrow progenitor cells: preventive effects of metformin. *Diabetes Res Clin Pract*. 2013; 101(2):177–186.
12. Bucala R, Makita Z, Koschinsky T, Cerami A, Vlassara H. Lipid advanced glycosylation: pathway for lipid oxidation in vivo. *Proc Natl Acad Sci U S A*. 1993;90(14):6434–6438.
13. Sykaras N, Iacopino AM, Marker VA, Triplett RG, Woody RD. Implant materials, designs, and surface topographies: their effect on osseointegration. A literature review. *Int J Oral Maxillofac Implants*. 2000;15(5):675–690.
14. Broggini N, McManus LM, Hermann JS, et al. Peri-implant inflammation defined by the implant-abutment interface. *J Dental Res*. 2006; 85(5):473–478.
15. Hanawa T. A comprehensive review of techniques for biofunctionalization of titanium. *J Periodontal Implant Sci*. 2011;41(6):263–272.
16. Souza JC, Barbosa SL, Ariza EA, et al. How do titanium and Ti6Al4V corrode in fluoridated medium as found in the oral cavity? An in vitro study. *Mater Sci Eng C Mater Biol Appl*. 2015;47:384–393.
17. Rupp F, Scheideler L, Rehbein D, Axmann D, Geis-Gerstorfer J. Roughness induced dynamic changes of wettability of acid etched titanium implant modifications. *Biomaterials*. 2004;25(7–8):1429–1438.
18. Di Iorio D, Traini T, Degidi M, Caputi S, Neugebauer J, Piattelli A. Quantitative evaluation of the fibrin clot extension on different implant surfaces: an in vitro study. *J Biomed Mater Res B Appl Biomater*. 2005; 74(1):636–642.
19. Rotaru H, Schumacher R, Kim SG, Dinu C. Selective laser melted titanium implants: a new technique for the reconstruction of extensive zygomatic complex defects. *Maxillofac Plast Reconstr Surg*. 2015; 37(1):1.
20. Mullen L, Stamp RC, Fox P, Jones E, Ngo C, Sutcliffe CJ. Selective laser melting: a unit cell approach for the manufacture of porous, titanium, bone in-growth constructs, suitable for orthopedic applications. II. Randomized structures. *J Biomed Mater Res B Appl Biomater*. 2010; 92(1):178–188.
21. Van der Stok J, Van der Jagt OP, Amin Yavari S, et al. Selective laser melting-produced porous titanium scaffolds regenerate bone in critical size cortical bone defects. *J Orthop Res*. 2013;31(5):792–799.
22. Traini T, Mangano C, Sammons RL, Mangano F, Macchi A, Piattelli A. Direct laser metal sintering as a new approach to fabrication of an isoelastic functionally graded material for manufacture of porous titanium dental implants. *Dent Mater*. 2008;24(11):1525–1533.
23. Mangano C, Raspanti M, Traini T, Piattelli A, Sammons R. Stereo imaging and cytocompatibility of a model dental implant surface formed by direct laser fabrication. *J Biomed Mater Res A*. 2009;88(3):823–831.
24. Marshall M, Oberhofer H, Staubesand J. Early micro- and macroangiopathy in the streptozotocin diabetic minipig. *Res Exp Med (Berl)*. 1980;177(2):145–158.
25. von Wilmowsky C, Stockmann P, Harsch I, et al. Diabetes mellitus negatively affects peri-implant bone formation in the diabetic domestic pig. *J Clin Periodontol*. 2011;38(8):771–779.
26. Fang K, Song W, Wang L, et al. Immobilization of chitosan film containing semaphorin 3A onto a microarc oxidized titanium implant surface via silane reaction to improve MG63 osteogenic differentiation. *Int J Nanomedicine*. 2014;9:4649–4657.
27. Jensen-Waern M, Andersson M, Kruse R, et al. Effects of streptozotocin-induced diabetes in domestic pigs with focus on the amino acid metabolism. *Lab Anim*. 2009;43(3):249–254.
28. Herrero-Climent M, Lazaro P, Vicente Rios J, et al. Influence of acid-etching after grit-blasted on osseointegration of titanium dental implants: in vitro and in vivo studies. *J Mater Sci Mater Med*. 2013;24(8): 2047–2055.
29. Frosch KH, Barvencik F, Viereck V, et al. Growth behavior, matrix production, and gene expression of human osteoblasts in defined cylindrical titanium channels. *J Biomed Mater Res A*. 2004;68(2):325–334.
30. Itala AI, Ylanen HO, Ekholm C, Karlsson KH, Aro HT. Pore diameter of more than 100 microm is not requisite for bone ingrowth in rabbits. *J Biomed Mater Res*. 2001;58(6):679–683.
31. Mangano C, De Rosa A, Desiderio V, et al. The osteoblastic differentiation of dental pulp stem cells and bone formation on different titanium surface textures. *Biomaterials*. 2010;31(13):3543–3551.
32. Thieme M, Wieters KP, Bergner F, et al. Titanium powder sintering for preparation of a porous functionally graded material destined for orthopedic implants. *J Mater Sci Mater Med*. 2001;12(3):225–231.
33. Zinger O, Anselme K, Denzer A, et al. Time-dependent morphology and adhesion of osteoblastic cells on titanium model surfaces featuring scale-resolved topography. *Biomaterials*. 2004;25(14):2695–2711.
34. Matena J, Gieseke M, Kampmann A, et al. Characterization of cell growth on titanium scaffolds made by selective laser melting for tissue engineering. *Biomed Tech (Berl)*. Epub 2013 Sep 7.
35. Ingber DE. Tensegrity II. How structural networks influence cellular information processing networks. *J Cell Sci*. 2003;116(Pt 8): 1397–1408.
36. Shibli JA, Mangano C, D'Avila S, et al. Influence of direct laser fabrication implant topography on type IV bone: a histomorphometric study in humans. *J Biomed Mater Res A*. 2010;93(2):607–614.